ELSEVIER

Chemical Geology 232 (2006) 67–86

CHEMICAL GEOLOGY
INCLUDING
ISOTOPE GEOSCIENCE

www.elsevier.com/locate/chemgeo

Opal as a U–Pb geochronometer: Search for a standard

Yuri Amelin [a,*], Malcolm Back [b]

[a] Geological Survey of Canada, 601 Booth St., Ottawa, ON, Canada K1A 0E8
[b] Department of Natural History, Earth Sciences, Royal Ontario Museum, 100 Queen's Park, Toronto, ON, Canada M5S 2C6

Received 9 March 2005; received in revised form 19 January 2006; accepted 11 February 2006

Abstract

We report structural, geochemical, and TIMS U–Th–Pb and U-series isotopic data for several samples of precious and common opal, which we tested as potential standards for ion microprobe and LA-ICPMS isotopic studies. The precious opals are low in U, contain high concentration of common Pb, and are not suitable for U–Pb age determinations. In contrast, all studied samples of common opal are enriched in uranium and contain sufficiently radiogenic Pb for precise calculations of $^{206}Pb/^{238}U$ and $^{207}Pb/^{235}U$ dates. Complications in the U–Pb systematics are due to the presence of ubiquitous unsupported ^{206}Pb, probably derived from initial excess ^{234}U and possibly other intermediate products of ^{238}U decay, elevated concentrations and possibly anomalous isotopic composition of initial Pb in some of the opals, and the presence of two opal generations of different ages in one of the samples. Despite these imperfections, two out of five studied common opals are acceptable as U–Pb and U-series standards, at least in the interim. The data obtained in this study can be used to guide further search for a better opal standard.

Keywords: Silica; Opal; Chalcedony; U–Pb; U-series disequilibrium; XRD

1. Introduction

Uranium–lead method is widely used for dating processes that fractionate U from Pb. Four groups of processes are well known to effectively fractionate these elements: magma crystallization (fractionation depends on compatibility of U and Pb in minerals), evaporation and condensation (fractionation due to higher volatility of Pb), dissolution and precipitation (fractionation due to higher solubility of oxidized U in water), and sub-solidus mineral growth during metamorphism. Successful application of U–Pb geochronometer depends on finding appropriate minerals that concentrate U and exclude Pb during their formation, but preserve radiogenic Pb and other decay products of uranium formed during the lifespan of the mineral. Crystallization of magma is successfully dated using a variety of igneous minerals enriched in U and depleted in Pb: zircon, baddeleyite, monazite and others. Volatility-related Pb–U fractionation makes it possible to date refractory meteorite components: chondrules and Ca–Al rich inclusions, as well as bulk meteorites depleted in volatile elements. Low mobility of Pb compared to mobility of U in oxidizing near-neutral pH water (Gaillardet et al., 2003) facilitates high U/Pb ratios in hydrogenic (water-laid) minerals such as calcite and amorphous silica.

* Corresponding author. Tel.: +1 613 995 3471; fax: +1 613 995 7997.
E-mail addresses: yamelin@nrcan.gc.ca (Y. Amelin), malcolmb@rom.on.ca (M. Back).

0009-2541/$ - see front matter © 2006 Elsevier B.V. All rights reserved.
doi:10.1016/j.chemgeo.2006.02.018

Table 1
Sample descriptions and X-ray diffraction data

Sample	Common or precious opal	Origin	Appearance	UV fluorescence	Material analyzed for X-ray diffraction (XRD)	XRD patterns	Classification based on XRD
E1989	Common	Kamloops Lake, British Columbia	Thin (<10 mm) layer of clear, colourless, optically homogeneous amorphous silica with botryoidal texture.	Brightness is relatively low and slightly variable at millimetre scale.	Two colourless transparent fragments with slight opalescence	Both fragments are basically X-ray amorphous. One of the films gave a hint of one very weak line at approximately 4 Å (identified visually), consistent with the opal-CT or opal-C.	Opal-A, with a possible small addition of opal-CT or opal-C
M21006	Common	Leo, Wyoming	Massive white translucent opal intersected by veins of clear opal. The thickness of the veins varies from 2–3 mm to less than 0.1 mm.	Both translucent matrix and clear veins are brightly fluorescent. Brightness is variable but does not correlate with veining	Four fragments: two colourless transparent (vein), and and two translucent (matrix)	All four films suggested relatively low degree of crystallinity (Fig. 2a,b) and matched the data for opal-CT of Graetsch (1994). Translucent variety shows slightly higher degree of crystallinity.	Opal-CT
M21277	Common	Humboldt County, Nevada	Massive yellowish opal, with no macroscopic heterogeneity visible in plain light. Microscopic netlike structure, clearly visible in thin shards of this opal in transmitted light, may suggest possible diatomite origin.	Relatively homogeneous bright fluorescence with some variation in brightness between broad (ca. 5–20 mm), approximately parallel zones.	Two visually identical milky translucent fragments	Very weak and diffuse diffraction patterns.	Opal-CT
BZ-VV	Common	Virgin Valley, Nevada	Similar to M21277. Previously studied by Zielinski (1982).	Similar to M21277	Not analyzed	Not analyzed	Not analyzed
HV-1	Common	Harper Valley, Nevada	Mostly massive translucent silica, which locally, grades into cloudy and opaque white varieties. Visually most heterogeneous sample among the studied common opals.	Relatively bright but variable.	Four fragments: (1) Translucent, slightly cloudy. (2) Colourless transparent. (3) Colourless, translucent to milky. (4) White, translucent.	(1) Well crystallized quartz pattern. (2) X-ray amorphous with no discernable lines. (3) Mixed pattern of well crystallized quartz with a weaker, more diffuse pattern of moganite. (4) Mixed pattern of crystalline quartz and cristobalite.	(1) Quartz (2) Opal-A (3) Quartz+moganite (4) Quartz+cristobalite
Assorted	Precious	Unknown	Green-red opalescence in plain light. Visually homogeneous.	None	Not analyzed	Not analyzed	Not analyzed
Bone	Precious	Unknown	Green-red opalescence in plain light. Shadow structure suggesting that it was formed by silicification of a bone.	None	One opalescent fragment	Very weak and diffuse diffraction patterns	Opal-CT
M42001	Precious	Australia	Green-red opalescence in plain light. Visually homogeneous.	None	One opalescent fragment	X-ray amorphous	Opal-A

U–Pb geochronology of hydrogenic minerals is relatively little developed compared to geochronology of igneous minerals, and has been mostly limited to carbonates. Amorphous silica may be an even more promising U–Pb and ^{230}Th–U geochronometer than carbonate minerals, because of its ability to concentrate uranium from water while effectively rejecting lead and thorium. First attempts to use opal ($SiO_2 \cdot nH_2O$) as a U–Pb geochronometer had shown its potential for dating Miocene and Pliocene hydrogeological events (Ludwig et al., 1980; Zielinski, 1982). U–Pb isotopic systems in amorphous silica were more extensively applied to study paleo-hydrology at Yucca Mountain—a proposed site for a high-level radioactive waste repository (Neymark et al., 2000, 2002; Wilson et al., 2003). Widespread occurrence of amorphous silica, together with high U concentrations and very low common Pb concentrations measured in this mineral in most cases, suggest that this mineral may eventually become as widely used U–Pb geochronometer as zircon.

A word about terminology, "Amorphous silica" is an extensive group of minerals with a wide variety of structures. In this paper, we use the names "opal" and "amorphous silica" as interchangeable synonyms, to include all structural varieties from truly amorphous to microcrystalline quartz. In the cases where structures are important, we use more specific names,

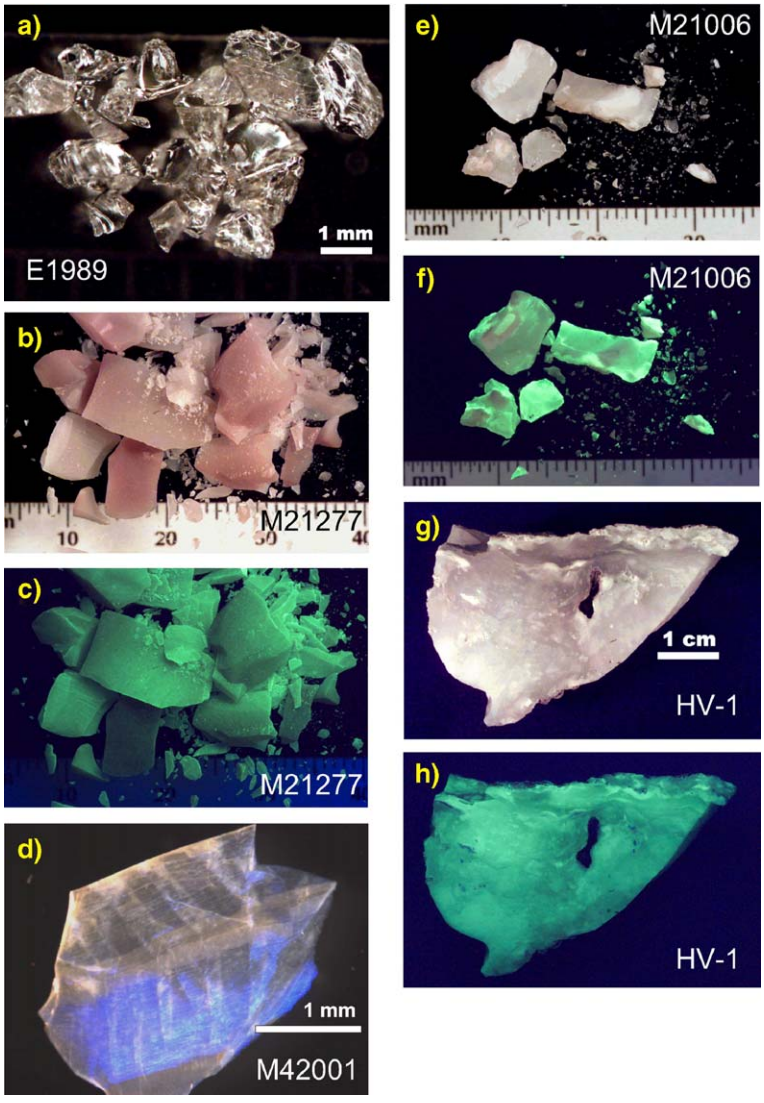

Fig. 1. Photographs of the studied opals in plain light (panels a, b, d, f, g) and in short-wave UV light (green fluorescence—panels c, f, h). (For interpretation of the references to colour in this figure legend, the reader is referred to the web version of this article.)

Table 2
Major and trace element concentrations

Sample	Na, ppm	Mg, ppm	K, ppm	V	Cr	Mn	As	Cu	Sr	Rb	Cd	Ba	La	Ce
E1989	17	96	na	520	240	410	350	150	840	252	<MDL	2500	8.2	16.0
M21006 clear	200	150	53	780	760	1300	<MDL	<MDL	16,000	210	93	6300	37	1000
M21006 translucent	350	860	92	2200	1200	2700	430	<MDL	16,700	580	<MDL	10,000	45	1400
M21277 fraction 1	110	400	250	12,000	na	22,000	710	1300	5300	na	115	640	1100	1400
M21277 fraction 2	110	380	240	13,000	na	23,000	710	1010	5300	na	118	810	1100	1200
BZ-VV	360	470	360	21,000	1900	13,000	2400	<MDL	6300	2000	830	<MDL	3500	3600
HV-1	180	23	170	1000	420	500	120	<MDL	2700	500	<MDL	2000	130	430
BONE	2000	72	na	200	270	17,000	1300	1070	13,300	26,000	150	45,000	420	880
M42001	1400	210	na	200	140	40,000	600	410	58,000	11,700	65	85,000	1200	3700

All concentrations are in ppb unless indicated otherwise.
<MDL—less than Mean Detection Limit.
na—not analyzed.

e.g. “opal-A”, “opal-CT”, for structural varieties of amorphous silica.

2. Need for a standard

In the studies mentioned above opal was analysed for U–Pb using isotope dilution—a technique that does not require a standard. However, this technique requires relatively large samples, which limits its application for deciphering history of commonly slowly formed, finely laminated opals. Growing use of U–Pb and U-series systems in opal includes microbeam analysis using laser ablation ICP-MS (Stirling et al., 2000) and ion microprobe (Paces et al., 2004; Nemchin et al., 2006). Both of these techniques require standards with composition and physical properties close to those of the analysed unknowns. Additional quantities of homogeneous opal are required for experimental studies to test stability of U–Th–Pb isotopic systems in opal and their change with structural modification of this mineral.

3. Requirements to the standard, and sample selection

In order to be datable with U–Pb and ^{230}Th–U methods with high precision and accuracy, a mineral should contain sufficiently high U and radiogenic Pb, low common Pb and ^{232}Th, and remain closed geochemical system since formation. In order to become a useful standard for U–Pb dating, the mineral in addition should be homogeneous in age, uranium content and structure, and should be available in sufficiently large amounts to be distributed among interested researchers at present and in the future. The requirements for a U-series standard are similar, but the condition of age homogeneity can be relaxed as long as the youngest phase of the mineral is sufficiently old to reach secular equilibrium in the ^{238}U decay chain.

Some of the requirements to the standards are obvious, and others are less so. The requirement of age uniformity (or the uniformity of radiogenic Pb/U ratios) is fundamental and needs no comments, but the requirements of uniform U content and low common Pb content may seem unnecessary. However, the requirement of uniform U content is important because variations in U content indicate changes in mineral growth conditions, which may be associated with changes in initial equilibrium, crystallinity, and other important parameters. Low content of common Pb is likewise important. If the standard is known to have low and uniform common Pb, then almost all common Pb detected in analysis is attributed to contamination in the analytical procedure (handling, gold coating, etc.). If, on the other hand, the content of common Pb in the standard is high and/or variable, and the isotopic compositions of “initial” and “procedural” common Pb differ, then subtraction of common Pb becomes more uncertain, and an additional error is introduced to the calculated radiogenic U/Pb ratios.

Concordance of U–Pb system is not strictly required for a U–Pb standard, but it is certainly beneficial. Concordance testifies that complicating factors, migration of U or Pb and fractionation of U-series nuclides, were absent. A mineral that was formed and existed in such conditions would have a homogeneous U–Pb system and would make a suitable standard. On the

Pr	Nd	Sm	Eu	Gd	Tb	Dy	Ho	Er	Yb	Lu	Th	U	U/Nd
1.9	7.1	1.5	1.1	2.2	0.56	4.3	1.2	5.9	13.1	2.8	2.3	1460	210
8.7	31	6.9	2.4	7.3	0.83	5.8	0.9	3.5	3.6	1.0	410	630,000	2100
9.8	33	5.7	2.3	5.0	0.63	3.8	0.59	2.3	3.3	0.6	430	300,000	9100
360	2000	580	65	840	180	1300	330	1050	1000	170	140	970,000	490
350	1900	550	63	800	170	1280	320	1010	970	160	120	1,130,000	600
850	3400	740	67	710	150	700	130	300	270	40	650	98,000	28
36	120	19	5.1	17.0	1.8	11.7	2.3	9.5	10.7	1.7	47	25,000	210
110	450	94	32	100	18	94	20	61	57	9.2	73	78	0.18
600	3040	700	240	650	130	670	130	380	300	44	43	42	0.014

contrary, discordance of U–Pb system indicates that U and/or Pb did migrate, or that U decay series were initially in disequilibrium. A mineral can still have homogeneous U/Pb ratios if migration of U and Pb, and initial fractionation in U-series, occurred uniformly on a scale larger than the size of the specimen. However, if a series of analyses yielded consistent U/Pb ratios but discordant U–Pb system or an evidence for initial disequilibrium, then the inference that the U/Pb ratios are homogeneous throughout the specimen requires assumption that migration and fractionation of elements occurred on a large scale, but additional fractionation on a sub-specimen scale was absent. This assumption is hard to validate, because migration and fractionation of elements are known to operate at various scales, from sub-micron to the entire magmatic or hydrothermal system. Moreover, the efficiency of fractionation can vary greatly with scale. Concordance of U–Pb system thus provides an additional support to the suitability of the mineral as a standard. The requirements of homogeneity and availability in large quantities disqualify, for example, Yucca Mountain opals (Neymark et al., 2000, 2002; Wilson et al., 2003) as potential U–Pb standards because they are small and their age may vary considerably between nearby occurrences of opal just a few millimetres apart. We have therefore searched for potential standards in the mineral collection of the Royal Ontario Museum (ROM), Toronto. Together with R. Ramik, we have examined several opal and chalcedony samples, looking for sufficiently large and visually homogeneous samples, preferably free of turbidity and inclusions. Since previous reports (Neymark et al., 2002) have shown that the brightness of green fluorescence of opal under short-wave UV illumination is roughly proportional to uranium concentration, we were also looking for samples with bright and uniform fluorescence.

We have selected three large (ca. 1–20 g) opal samples from the mineral collection of the ROM (E1989, M21006, M21277). One sample (BZ-VV) was provided by R. Zielinski, U.S. Geological Survey (USGS). The sample HV-1, provided by L. Neymark, was collected at Harper Valley, S. Nevada. These samples are collectively referred to as "common opal" to distinguish them from "precious opal" that shows opalescence. We selected four samples of precious opal from the ROM mineral collection. A brief description of samples is given in Table 1. Photographs of selected samples are shown in Fig. 1.

4. Methods

4.1. X-ray diffraction

Mineral phases present in the various opal samples were investigated using powder X-ray diffraction at the Department of Natural History, Earth Sciences, Royal Ontario Museum. Most films were exposed in a 114.6 mm diameter Gandolfi camera using a ball mount for 18 h, with a few runs at 24 h, while a few exposures were run in a 114.6 mm diameter Debeye-Scherrer camera using a powder on fibre mount. The generator used was a Philips P1120/60, equipped with a Thales D7600GXRTC, MC61-04 fine-focus, copper, 60 kV, 1500 W, X-ray tube, running at 35 kV, and 20 mA. Cu/Ni radiation was used for all films, and the films were scanned using an optical scanner, calibrated for

Table 3
U–Pb data

Sample	Fraction #	Fraction description (1)	Sample wt. mg	U ppm	Th ppb	Total Pb ppb	$^{238}U/^{204}Pb$ (2)	2σ %err	$^{206}Pb/^{204}Pb$ (3)	$^{206}Pb/^{204}Pb$ (2)	2σ %err	$^{207}Pb/^{204}Pb$ (2)	2σ %err
E1989	1	Clear	7.130	8	0.129	17	402,000	7.3	762	1030	7.1	59.9	5.4
	2	Clear less fluor	5.870	2	0.015	7	81,200	5.9	199	250	5.5	24.51	2.4
	3	Clear	1.660	7	na	16	7,400,000	2500	614	19,200	2540	814	2490
	4	Clear	1.678	6	na	19	72,000	27	160	204	25	23.5	9.6
	5	Clear	0.398	19	na	45	53,400	140	526	1360	134	75	108
	6	Clear	0.382	18	na	43	880,000	240	593	2260	238	114	208
M21006	7	Transparent vein	1.640	579	36	222	2,760,000	3.0	1050	1190	2.9	69.1	2.4
	8	Transparent vein	0.582	667	na	268	8,700,000	86	1870	3800	85.2	190	79
	9	Transparent vein	0.568	676	na	309	7,900,000	79	2020	3980	78.2	196	72
	10	Transparent vein	0.148	593	na	237	1,700,000	74	378	700	71.9	47	50
	11	Transparent vein	0.134	658	na	252	1,600,000	68	347	620	65.7	43	44
	12	Transluc matrix	2.100	281	355	376	414,000	0.92	580	600	0.82	41.9	0.67
	13	Transluc matrix	0.561	266	na	269	1,490,000	38	1110	1620	37.5	89	32
	14	Transluc matrix	0.617	243	na	356	470,000	12	621	710	11.7	46.7	8.1
	15	Transluc matrix	0.327	276	na	570	80,800	3.5	129	134	2.96	20.81	1.0
	16	Transluc matrix	0.392	269	na	428	510,000	18	692	850	18.0	53.1	13
M21277	17	Translucent	0.019	565	na	282	420,000	160	81	180	137	22.1	48
	18	Translucent	0.035	1016	na	505	560,000	60	158	260	55.4	25.3	24
	19	Translucent	0.025	809	na	372	810,000	150	142	360	146	29.4	75
	20	Translucent	0.012	890	na	433	580,000	105	137	270	97.3	24.7	40
	21	Translucent	0.030	881	na	460	440,000	64	125	200	57.7	23.2	22
	22	Translucent	0.014	1135	na	504	990,000	240	131	440	229	32.5	127
	23	Translucent	0.606	1047	156	572	357,000	1.4	161	166	0.96	21.47	0.38
	24	Translucent	0.232	1042	179	445	1,030,000	8.0	361	438	7.62	31.4	4.0
	25	Translucent	0.563	965	159	559	306,000	2.2	142	146	0.95	20.74	0.37
	26	Translucent	0.479	1018	177	451	749,000	3.1	297	319	2.72	26.92	1.23
	27	Translucent	0.406	998	189	480	539,000	2.6	224	238	2.31	23.89	0.92
	28	Translucent	0.423	888	184	397	762,000	4.2	299	330	3.59	27.24	1.63
	29	Translucent	0.483	1045	185	589	325,000	1.6	148	153	1.08	20.94	0.38
	30	Translucent	0.812	880	177	430	487,000	1.5	207	214	1.21	23.03	0.54
BZ-VV	31	Translucent	0.980	841	173	401	736,000	0.60	331	339	0.55	28.16	0.33
	32	Translucent	1.041	748	228	400	446,000	0.43	211	214	0.35	23.26	0.21
	33	Translucent	1.712	583	276	332	365,000	4.8	178	180	0.24	21.88	0.18
	34	Translucent	0.758	852	208	415	693,000	0.75	315	325	0.66	27.50	0.39
	35	Translucent	0.652	888	176	422	780,000	0.90	348	362	0.83	28.84	0.48
HV1	36	Relatively clear	1.817	19.7	na	21	103,000	11	64	69.1	8.15	17.79	1.8
	37	Relatively clear	0.665	26.0	na	26	115,000	27	64	75.9	19.5	18.40	4.8
	38	Slightly cloudy	0.642	20.0	na	44	41,000	13	46	48.6	7.78	16.94	1.6
	39	White	0.644	29.8	na	26	139,000	29	69	84	21.80	18.40	5.2
Assorted	40	Precious opal	2.442	0.34	1250	5730	3.76	3.3	18.747	18.788	0.18	15.621	0.23
Assorted	41	Precious opal	3.141	0.38	1596	1596	15.2	1.5	18.724	18.763	0.13	15.615	0.17
"Bone"	42	Precious opal	6.065	0.033	62.7	1100	1.93	2.2	18.489	18.528	0.17	15.640	0.21
M42001	43	Precious opal	3.016	0.026	18.8	242	6.80	1.3	18.677	18.705	0.24	15.614	0.27

Sample	Rho 238/4–6/4 (4a)	Rho 235/4–7/4 (4b)	$^{208}Pb/^{204}Pb$ (2)	2σ %err	$^{207}Pb/^{235}U$ (5)	2σ %err	$^{206}Pb/^{238}U$ (5)	2σ %err	Rho 6/38–7/35 (4c)	$^{207}Pb/^{235}U$ date Ma (6)	2σ err Ma	$^{206}Pb/^{238}U$ date Ma (7)	2σ err Ma
E1989	0.999	0.973	41.5	1.7	.01516	0.58	.002511	0.33	0.57	15.28	.09	16.165	0.053
	0.996	0.913	39.4	1.6	.01509	2.2	.002853	0.64	0.30	15.20	.33	18.36	0.12
	1.000	0.977	65	1140	.01488	5.0	.00259	2.4	0.55	15.00	.75	16.67	0.40
	0.996	0.934	37.4	2.6	.01498	5.8	.00258	2.5	0.50	15.10	.88	16.59	0.42
	1.000	0.974	49.9	38	.01526	4.0	.00250	2.0	0.57	15.38	.61	16.12	0.32
	1.000	0.975	62.7	102	.01550	3.9	.00255	1.9	0.57	15.62	.61	16.39	0.32
M21006	0.987	0.961	38.94	1.1	.002678	0.61	.000425	0.49	0.80	2.716	.017	2.741	0.014
	1.000	0.976	40.3	11	.002751	1.2	.000438	0.94	0.81	2.789	.033	2.824	0.027
	1.000	0.976	41.3	12	.003140	1.4	.000500	1.3	0.90	3.184	.045	3.224	0.040
	1.000	0.969	39.8	9.3	.00252	4.0	.000402	2.0	0.57	2.56	.10	2.591	0.051
	1.000	0.968	38.4	7.2	.00241	4.1	.000382	2.0	0.57	2.44	.10	2.459	0.050
	0.919	0.869	39.02	0.96	.00875	0.60	.001403	0.39	0.58	8.846	.053	9.041	0.035
	1.000	0.974	40.2	4.9	.00676	1.0	.001077	0.70	0.71	6.839	.071	6.939	0.048
	0.997	0.966	39.32	1.9	.00916	1.4	.001478	0.98	0.73	9.25	.13	9.523	0.093
	0.974	0.866	38.26	0.45	.00884	3.3	.001424	0.91	0.24	8.93	.29	9.170	0.084
	0.999	0.970	41.03	2.7	.01013	1.1	.001624	0.68	0.67	10.24	.11	10.459	0.071
M21277	0.996	0.927	39.0	17	.00210	35	.000387	15	0.48	2.13	.74	2.50	0.37
	0.998	0.945	38.9	6.6	.00240	9.7	.000427	4.2	0.51	2.43	.23	2.75	0.12
	0.999	0.957	41.3	22	.00234	17.1	.000423	7.6	0.51	2.37	.41	2.73	0.21
	0.998	0.943	36.4	10	.00214	17.5	.000427	7.0	0.47	2.17	.38	2.75	0.19
	0.996	0.934	39.5	7	.00237	13.1	.000419	5.6	0.50	2.40	.31	2.70	0.15
	0.999	0.962	40.2	31	.00236	21.7	.000423	9.7	0.51	2.39	.52	2.72	0.26
	0.785	0.669	38.20	0.28	.002259	1.9	.000412	1.0	0.39	2.291	.043	2.654	0.027
	0.996	0.978	38.71	0.81	.002124	1.3	.000409	0.72	0.53	2.155	.028	2.634	0.019
	0.497	0.402	38.31	0.30	.002304	2.7	.000415	2.0	0.67	2.337	.063	2.677	0.054
	0.921	0.897	38.45	0.34	.002080	1.5	.000401	1.3	0.79	2.110	.032	2.587	0.032
	0.970	0.910	38.39	0.35	.002115	1.5	.000407	0.73	0.37	2.145	.032	2.620	0.019
	0.915	0.895	38.37	0.38	.002101	1.9	.000408	1.7	0.87	2.131	.041	2.628	0.045
	0.777	0.663	38.23	0.27	.002255	2.1	.000412	1.2	0.41	2.288	.048	2.655	0.031
	0.879	0.775	38.41	0.38	.002098	1.6	.000401	0.83	0.41	2.128	.034	2.584	0.021
BZ-VV	0.963	0.853	38.86	0.28	.002349	0.79	.000436	0.30	0.74	2.382	.007	2.808	0.022
	0.864	0.664	38.76	0.25	.002363	1.3	.000438	0.47	0.76	2.397	.011	2.824	0.035
	0.054	0.040	38.81	0.22	.00236	5.0	.000440	4.8	0.97	2.40	.12	2.84	0.14
	0.925	0.822	39.05	0.38	.002365	0.88	.000441	0.39	0.72	2.398	.009	2.844	0.025
	0.968	0.883	38.71	1.8	.002336	0.80	.000440	0.33	0.71	2.369	.008	2.835	0.023
HV1	0.968	0.760	39.16	1.3	.00289	11	.000488	3.0	0.33	2.93	.31	3.15	0.096
	0.974	0.819	39.29	3.0	.00332	15	.000497	6.1	0.48	3.36	.51	3.20	0.19
	0.939	0.624	39.24	1.5	.00440	19	.000728	4.9	0.32	4.45	.82	4.69	0.23
	0.978	0.822	38.64	3.0	.00274	16	.000467	6.0	0.45	2.78	.45	3.01	0.18
Assorted	0.055	0.050	38.70	0.24									
Assorted	0.084	0.080	38.63	0.20									
"Bone"	0.081	0.077	38.35	0.26									
M42001	0.189	0.180	38.51	0.30									

intensity and peak position using external standards of silicon (640a) and quartz. Structural varieties of silica were identified by pattern matching using the JADE 6 package by Materials Data Inc., and the ICDD PDF-2, release 2002, powder diffraction file. All patterns and data were also visually compared against the data published by Graetsch (1994).

4.2. Major and trace element concentrations

Concentrations of some major and trace elements in opal samples (Table 2) were determined by inductively coupled plasma mass-spectrometer (ICP-MS) Plasma-Quad-III™ at the USGS (Denver Federal Center, the Environmental Science Team of the Yucca Mountain Project Branch of the Water resources Discipline of the USGS). Samples were dissolved overnight in concentrated HF, dried down and re-dissolved in HNO_3. Samples were introduced into the ICP-MS at the rate of 0.8 ml/min by means of 9/9SS Meinhardt™ ultrasonic nebulizer. Typical RF forward power during analyzes was about 1350 W and run times were about 2.5 min per sample. A set of ICP-MS grade element standards was used for the calibration of the ICP-MS and 2σ errors of the reported trace element concentrations are about 10%.

4.3. Isotopic analyses

Most U–Pb analyses were performed at the Jack Satterly Geochronology Laboratory, ROM, using techniques described by Neymark et al. (2000, 2002) and Wilson et al. (2003) on a VG-354 thermal ionization mass spectrometer. Additional fractions (#23–30, Table 3) from the sample M21277 were analyzed for U–Pb at the Geological Survey of Canada using the same sample preparation and chemical separation procedures as at the ROM, and a two-step quasi-static multicollector analysis procedure on a Triton™ thermal ionization mass spectrometer. The ^{204}Pb peak was measured in the SEM channel, whereas the ^{205}Pb peak was measured in a Faraday cup in the first field position, and in the SEM in the second field position. The SEM gain was calculated in each scan and was used for correction of the ^{204}Pb signal. Using high-efficiency silica gel (Gerstenberger and Haase, 1997) allowed analyzing these small Pb loads, which contained 4–14 pg of ^{207}Pb, using Faraday collectors. The fractions were spiked with a mixed ^{205}Pb–^{230}Th–^{235}U tracer, calibrated against the same set of standard solutions (Amelin and Zaitsev, 2002) as the ^{205}Pb–^{229}Th–^{233}U–^{236}U tracer used for opal analyses at the Jack Satterly Laboratory. Analytical blanks were 1.5 ± 1.0 pg for Pb and 0.1 ± 0.1 pg for U.

The techniques used for U-series analyses at the USGS and at the ROM were described by Neymark and Paces (2000) and Neymark et al. (2000).

Data reduction is similar to those previously used at the Jack Satterly Geochronology Laboratory (Amelin et al., 1997). Isochron regressions and weighted averages with their error limits are calculated using Isoplot-Ex version 3.00 (Ludwig, 2003). Error limits are 95% confidence intervals for isochrons and weighted averages. Errors of the isotopic ratios and of other values mentioned in the text are 2ó of the mean, unless indicated otherwise.

4.4. Correction for common Pb in U–Pb date calculations

The Pb isotopic compositions of the common opals are sufficiently radiogenic to calculate ^{206}Pb∗/^{238}U and ^{207}Pb∗/^{235}U dates. In the following presentation of U–Pb data we use both “radiogenic” (initial-Pb corrected) ^{207}Pb∗/^{235}U and ^{206}Pb∗/^{238}U ratios calculated assuming average modern continental crustal Pb (Stacey and Kramers, 1975), and U–Pb isochrons, which do not involve correction for a priori known initial Pb. The U–Pb date calculations from single analysis (model date calculation) rely on accurate determination of the isotopic composition of initial Pb in the opals—a crucial parameter for the samples that contain only moderately radiogenic Pb. The most direct and accurate approach is using Pb isotopic composition in low U/Pb minerals cogenetic with the opal, e.g. calcite and Mn-crusts (Neymark and Amelin, 2002). This option is not available in this study because the chosen samples are pure opal, free of intergrowths with other minerals. An alternative way

Notes to Table 3:
(1) Fractions marked “less fluor” consist of fragments with lower brightness of fluorescence in short-wave UV light than other fractions from the same sample.
(2) Corrected for fractionation, spike and procedure blank.
(3) Measured ratio, no corrections applied.
(4) Error correlation between ^{238}U/^{204}Pb and ^{206}Pb/^{204}Pb (a), ^{235}U/^{204}Pb and ^{207}Pb/^{204}Pb (b), and ^{235}U/^{207}Pb* and ^{238}U/^{206}Pb* (c).
(5) Corrected for fractionation, spike, blank and initial common Pb (modern values in the Stacey and Kramers (1975) model).(6) Dates calculated assuming initial secular equilibrium in U decay chains.na—not analyzed.Blank cells—age cannot be calculated because all Pb in the fraction is common Pb.

of estimating initial Pb composition is plotting series of analyses of co-genetic samples (or fractions from the same sample) in $^{238}U/^{204}Pb$–$^{206}Pb/^{204}Pb$ and $^{235}U/^{204}Pb$–$^{207}Pb/^{204}Pb$ isochron diagrams. Intersections of these isochrons with *Y*-axis give estimates of initial Pb. These estimates are accurate if the isochron model assumptions of closed system and uniform age and initial Pb are satisfied, and if the decay chains of U isotopes are initially in secular equilibrium. Fulfillment of these assumptions is indicated by the co-linearity of the analytical points within error (true isochrons rather than "errorchrons"), and by agreement of the dates yielded by $^{238}U/^{204}Pb$–$^{206}Pb/^{204}Pb$ and $^{235}U/^{204}Pb$–$^{207}Pb/^{204}Pb$ isochrons.

5. Results

5.1. Structures and degrees of crystallinity

Structures and degrees of crystallinity of common opal samples E1989, M21006, M21277, HV1 and two

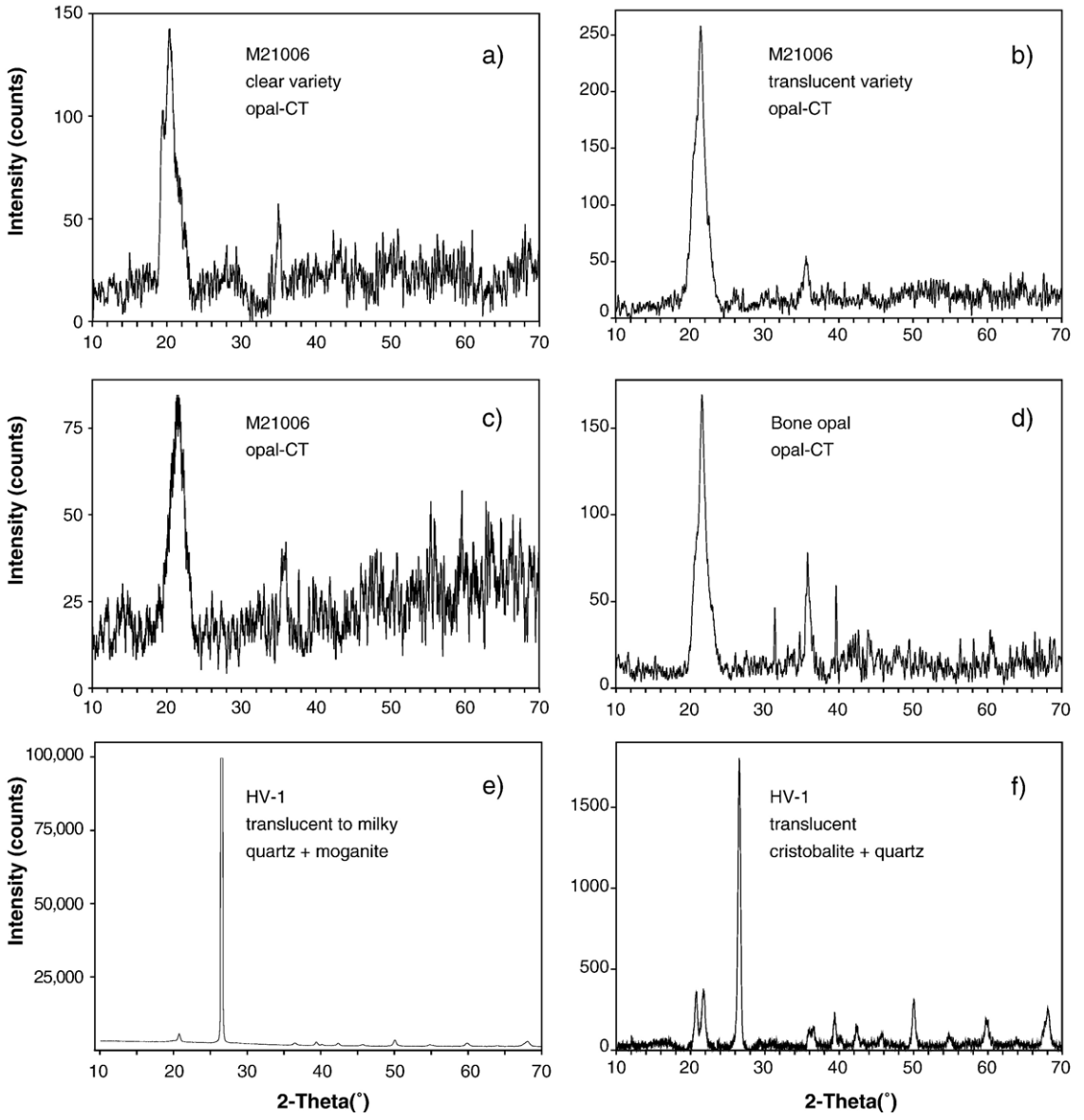

Fig. 2. Representative X-ray diffraction patterns of the opals. Structural varieties of silica were identified by pattern matching using the JADE 6 package by Materials Data Inc., and the ICDD PDF-2, release 2002, powder diffraction file. The differences in *Y*-axis scales among the samples reflect the variations in overall crystallinity: the most crystalline samples (two fractions of HV-1—e, f) contain intensive and narrow peaks, and have the highest ratio of the most intensive peak to noise. The *X*-axis scale is identical for all samples.

precious opal samples: M42001 and "Bone opal" were studied using X-ray diffraction. Representative X-ray diffraction patterns for the opals showing some crystallinity are shown in Fig. 2. The diffraction pattern for the sample E1989 (not included in Fig. 2) shows no peaks at all, indicating this sample is amorphous (opal-A). Detailed description of XRD patterns is presented in Table 1. The samples M21277 and M21006 show incipient crystallinity (opal-CT), whereas the sample HV-1 is more crystalline (contains quartz, cristobalite

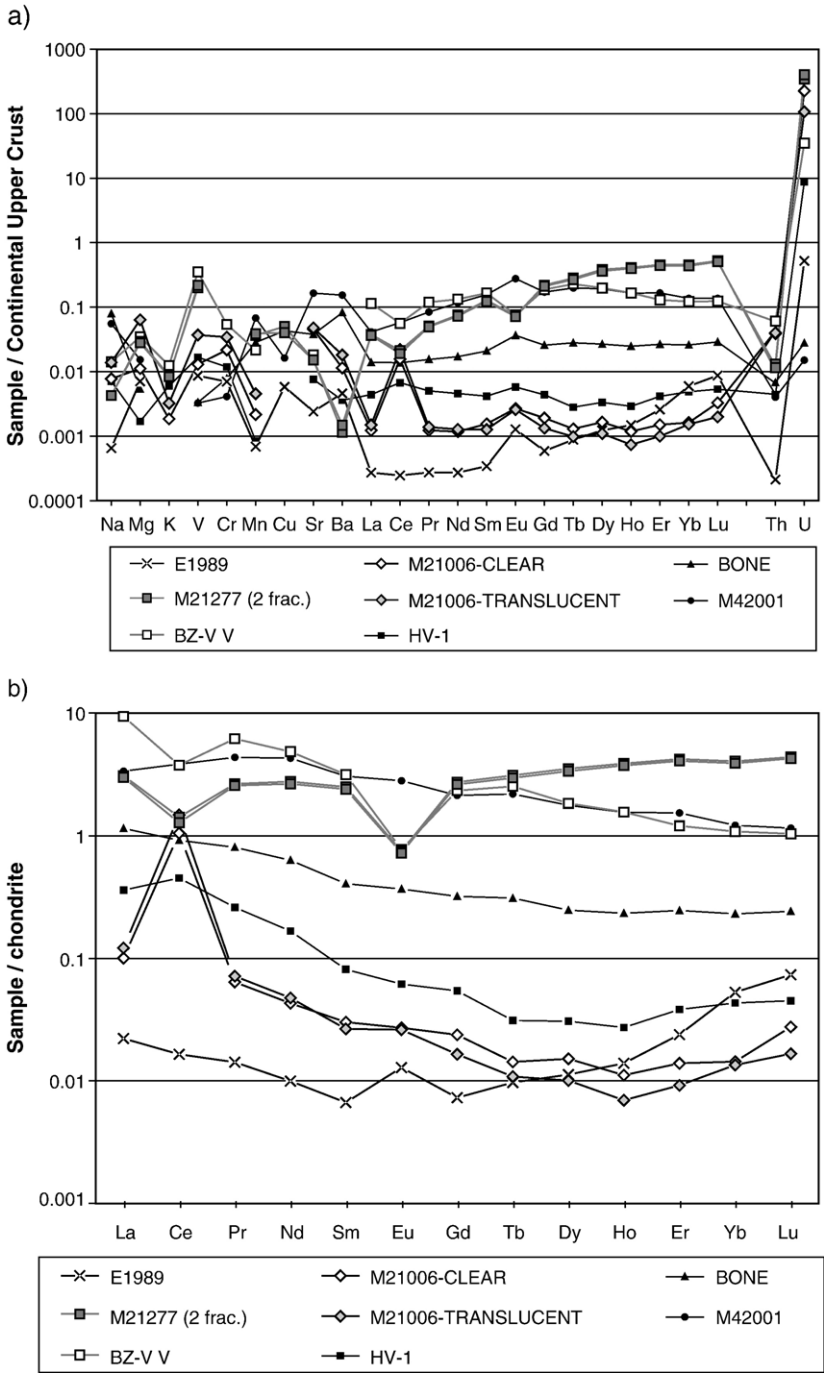

Fig. 3. Chemical composition of the studied opals. (a) Abundances of major and trace elements in the opals, normalized to the average concentration in continental upper crust (Taylor and McLennan, 1985). (b) Chondrite-normalized REE concentrations in the opals.

and moganite-fibrous microcrystalline silica; Flörke et al., 1984; Miehe and Graetsch, 1992).

5.2. Major and trace element compositions

Concentrations of Mg, K, Na, V, Cr, Mn, Cu, Sr, Ba and Th (Table 2) in the opals vary from 0.0003 to 0.3 of average upper crustal abundances of these elements (Fig. 3a). The opals M21277, BZ-VV and two precious opals have higher concentrations of most elements, whereas the opal E 1989 is more depleted in most elements.

REE abundances in the opals, shown as chondrite-normalized values in Fig. 3b, also vary within three orders of magnitude. Europium anomalies vary from slightly positive (E1989) to strongly negative (M21277, BZ-VV). Cerium anomalies are observed in the opals M21277 and BZ-VV (slightly negative) and M21006 (strongly positive), and are absent in other opals. Two visually distinct phases of the sample M21006, translucent matrix and clear veins, have nearly identical abundances of REE and almost all other elements.

The most prominent geochemical anomaly observed in all samples of common opal is enrichment in uranium relative to average upper crust (Fig. 3a) as compared to depletion in all other measured elements. In contrast, the precious opals are not enriched in uranium: their crust-normalized U abundances are similar to crust-normalized REE abundances in the same samples.

A contrast between common and precious opal is clearly seen in Fig. 4a,b, where the concentrations of Th and ^{204}Pb are plotted against the concentration of U. The ^{238}U/^{204}Pb values (Fig. 4a) range in the common opals between 41,000 and 8,700,000 (median 489,000), whereas in the precious opals these ratios are between 1.9 and 15.2 (median 5.3). U/Th ratios (Fig 4b) are also much higher in the common opals than in the precious opals.

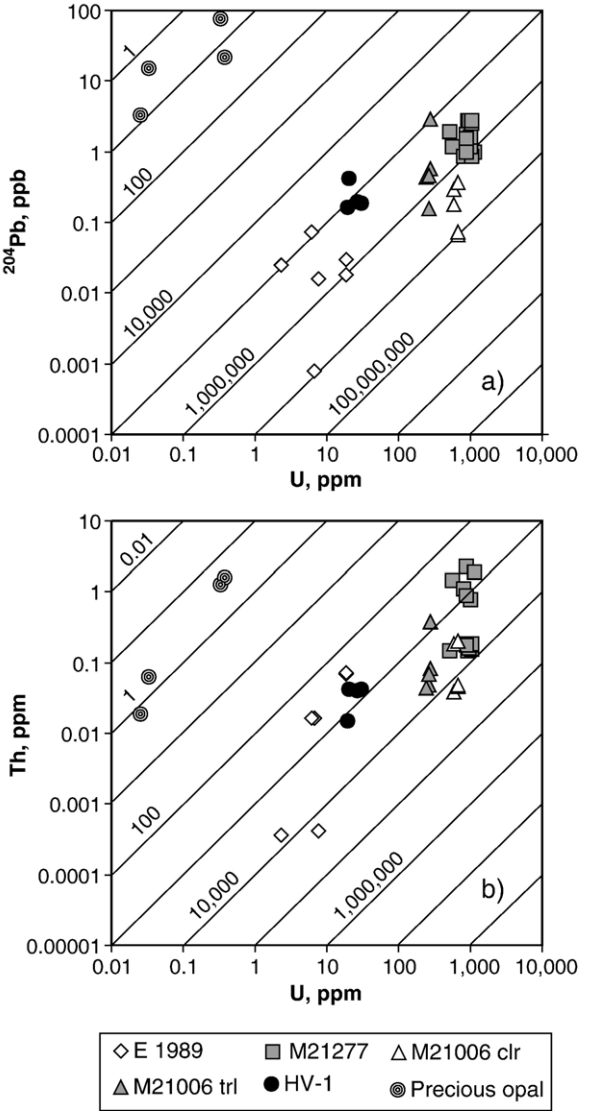

Fig. 4. Concentrations of U, Th, and ^{204}Pb in the studied opals. Diagonal lines show constant U–^{204}Pb and U–Th ratios; the lines are labelled with the values of respective ratios.

5.3. U–Pb data

The U–Pb data show elevated U concentrations and radiogenic Pb isotopic composition in the common opal samples and low U content and unradiogenic Pb isotopic composition in precious opal samples (Table 3). Four to fourteen fractions were analyzed from each sample of common opal. Fractions were selected to represent the variations in degree of transparency and in brightness of fluorescence under short wave UV illumination.

The sample E1989 is homogeneous in visible light but shows variation in the brightness of fluorescence. Six fractions have relatively low uranium concentrations of 2–19 ppm, the lowest concentration being observed in the low-fluorescence fraction. Despite the relatively low U content, the ^{238}U/^{204}Pb ratios are high, and Pb isotopic ratios are highly radiogenic. U–Pb analyses of all six fractions give discordant ages and plot above concordia (Fig. 5a). This inverse discordance can be caused by anomalous isotopic composition of initial Pb. Alternatively, it can be caused by the presence of variable amounts of unsupported ^{206}Pb produced by decay of excess intermediate products of ^{238}U decay: ^{234}U and possibly ^{226}Ra and ^{222}Rn. The possible presence of anomalous initial Pb is tested by plotting the data in ^{238}U/^{204}Pb–^{206}Pb/^{204}Pb and ^{235}U/^{204}Pb–^{207}Pb/^{204}Pb

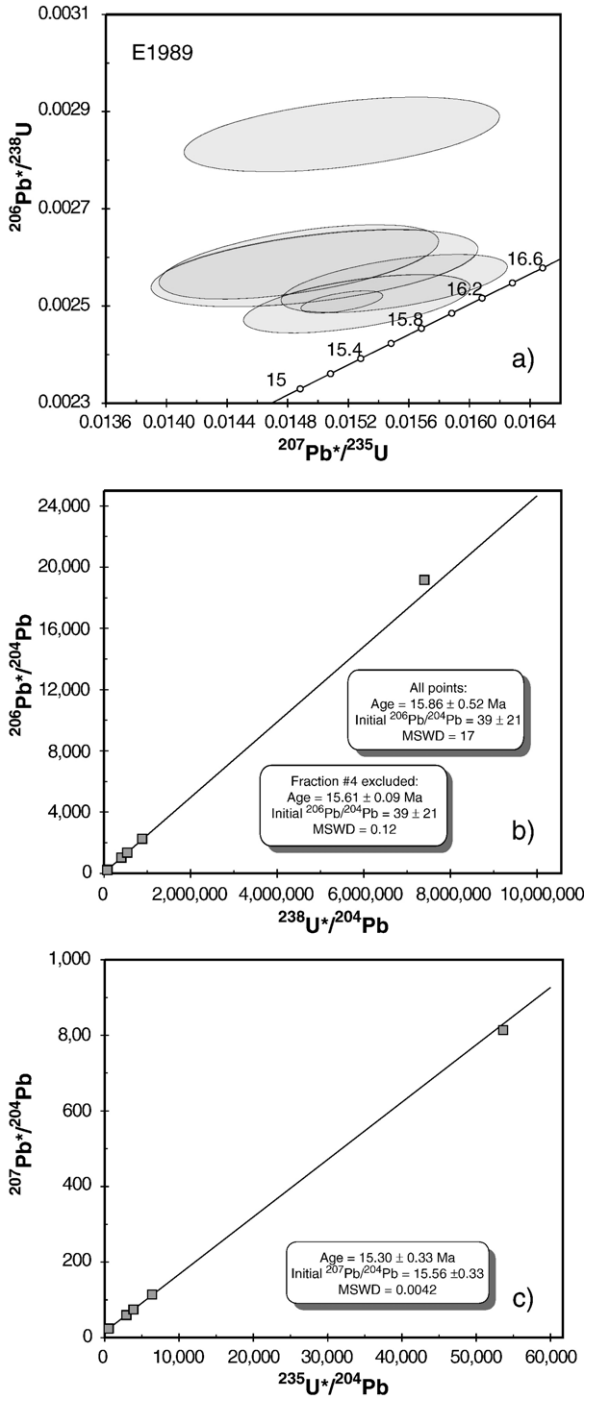

Fig. 5. U–Pb data for the opal E1989. (a) Concordia plot (asterisks denote radiogenic Pb hereafter). Error ellipses are 2σ. (b) $^{238}U/^{204}Pb$–$^{206}Pb/^{204}Pb$ and c) $^{235}U/^{204}Pb$–$^{207}Pb/^{204}Pb$ isochron diagrams. Due to very low content of ^{204}Pb, close to the analytical blank level, the errors of $^{238}U/^{204}Pb$ and $^{206}Pb/^{204}Pb$ (as well as $^{235}U/^{204}Pb$ and $^{207}Pb/^{204}Pb$) are large, variable and extremely strongly correlated (see Table 3). Error ellipses are therefore not plotted for clarity. Errors and their correlations are, however, taken into account in isochron regressions.

isochron diagrams (Fig. 5b,c). The $^{238}U/^{204}Pb$–$^{206}Pb/^{204}Pb$ "errorchron" (Fig. 5b) has large MSWD = 17, and yields the date of 15.86 ± 0.52 Ma and the initial $^{206}Pb/^{204}Pb = 39 \pm 21$. Excluding the point #4 containing the least radiogenic Pb (Table 3) produces an isochron without excess scatter (MSWD = 0.12), which yields more precise date of 15.61 ± 0.09 Ma and initial $^{206}Pb/^{204}Pb = 53.6 \pm 3.0$. This $^{206}Pb/^{204}Pb$ is much higher than the range of values in the modern continental crust (e.g. Stacey and Kramers, 1975; Kramers and Tolstikhin, 1997). The $^{235}U/^{204}Pb$–$^{207}Pb/^{204}Pb$ isochron (Fig. 5c) yields the date of 15.30 ± 0.33 Ma and the initial $^{207}Pb/^{204}Pb = 15.56 \pm 0.33$. The latter value agrees very well with the $^{207}Pb/^{204}Pb$ value of the modern continental crust.

U–Pb analyses of the sample M21006 were performed on five fractions from each of the two distinct varieties of opal: translucent "matrix" opal comprising 80–90% of the sample, and clear "vein" opal. U–Pb data show bimodal age distribution in the concordia diagram (Fig. 6a): the matrix opal yields $^{206}Pb^*/^{238}U$ and $^{207}Pb^*/^{235}U$ dates of 6.8–10.5 Ma, whereas the vein opal yields the dates of 2.4–3.2 Ma (Table 3). In each group, both $^{206}Pb^*/^{238}U$ and $^{207}Pb^*/^{235}U$ dates vary well outside of the analytical errors. U–Pb data for the matrix opal plot clearly above concordia; the discordance of the vein opal data is smaller but still significant for three more precise analyses (points #7–9, Table 3). Uranium concentration is relatively uniform within each age group, and is about 2–2.5 times higher in the vein opal than in the matrix opal. High uranium concentrations of >240 ppm in both groups, combined with low common Pb content, produced very high $^{238}U/^{204}Pb$ ratios (all fractions of vein opal yielded $^{238}U/^{204}Pb > 1{,}000{,}000$) and allowed high precision of U–Pb dates. The U–Pb data confirm that translucent and clear varieties are indeed two distinct age generations of opal. The younger vein opal probably precipitated at ca. 2.5 Ma on fractured 9–11 Ma matrix opal. The spread of U–Pb dates in both young and old groups along the same trend in the concordia diagram (Fig. 6a) suggests that the clear opal was formed, at least in part, by substitution of the old translucent opal. The data plotted in the $^{238}U/^{204}Pb$–$^{206}Pb/^{204}Pb$ and $^{235}U/^{204}Pb$–$^{207}Pb/^{204}Pb$ isochron diagrams (Fig. 6b,c) do not form a single linear array, but plot along separate lines with different slopes thus confirming age dichotomy. The initial Pb isotopic ratios shown by the isochron intercepts cannot be considered meaningful, because they are very imprecise and may be biased due to age variability in both translucent and clear opal samples.

Fourteen fractions of the opal M21277, varying in size from 0.012 mg to 0.812 mg, were analyzed for U–Pb. Uranium concentrations, from 565 to 1135 ppm, are high and relatively uniform. Pb isotopic ratios are relatively radiogenic, but not as high as in the sample M21006. All analyses are inversely discordant (Fig. 7a). Six smaller fractions weighing 0.014–0.030 mg (Table 3) were analyzed in order to test the homogeneity of the

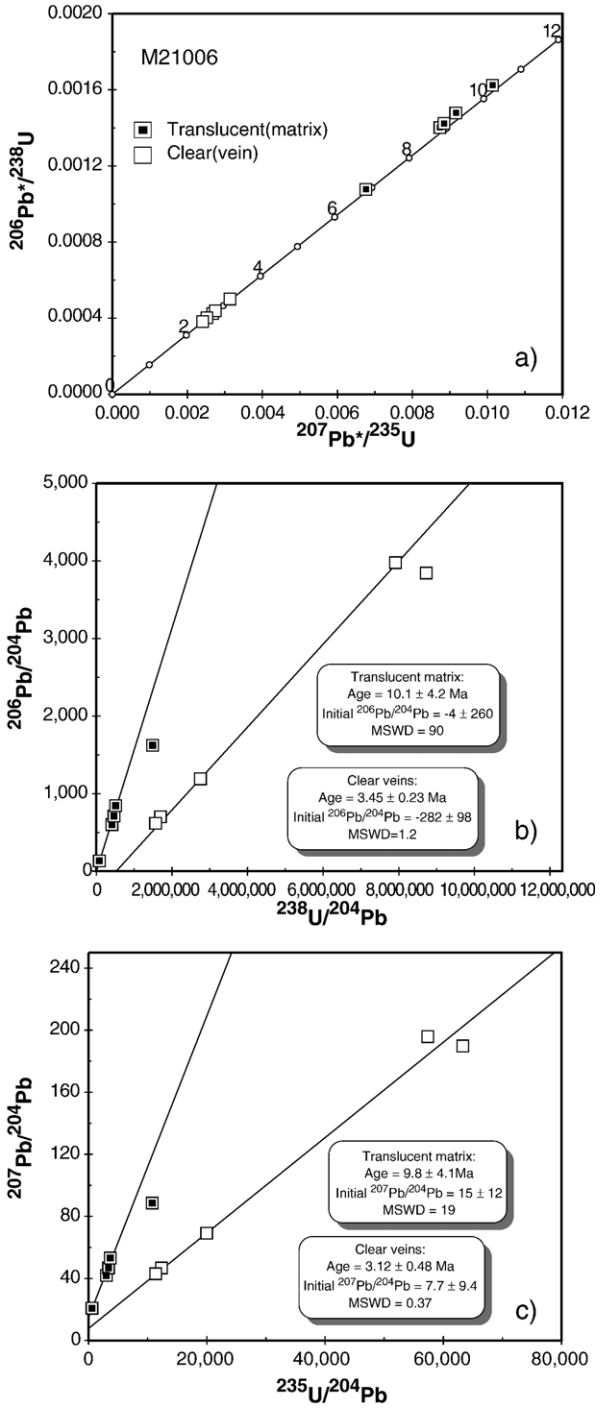

Fig. 6. U–Pb data for the opal M21006. (a) Concordia plot. (b) $^{238}U/^{204}Pb$–$^{206}Pb/^{204}Pb$ and (c) $^{235}U/^{204}Pb$–$^{207}Pb/^{204}Pb$ isochron diagrams. In all diagrams, 2σ error ellipses are smaller than the plotting symbols and are therefore not shown.

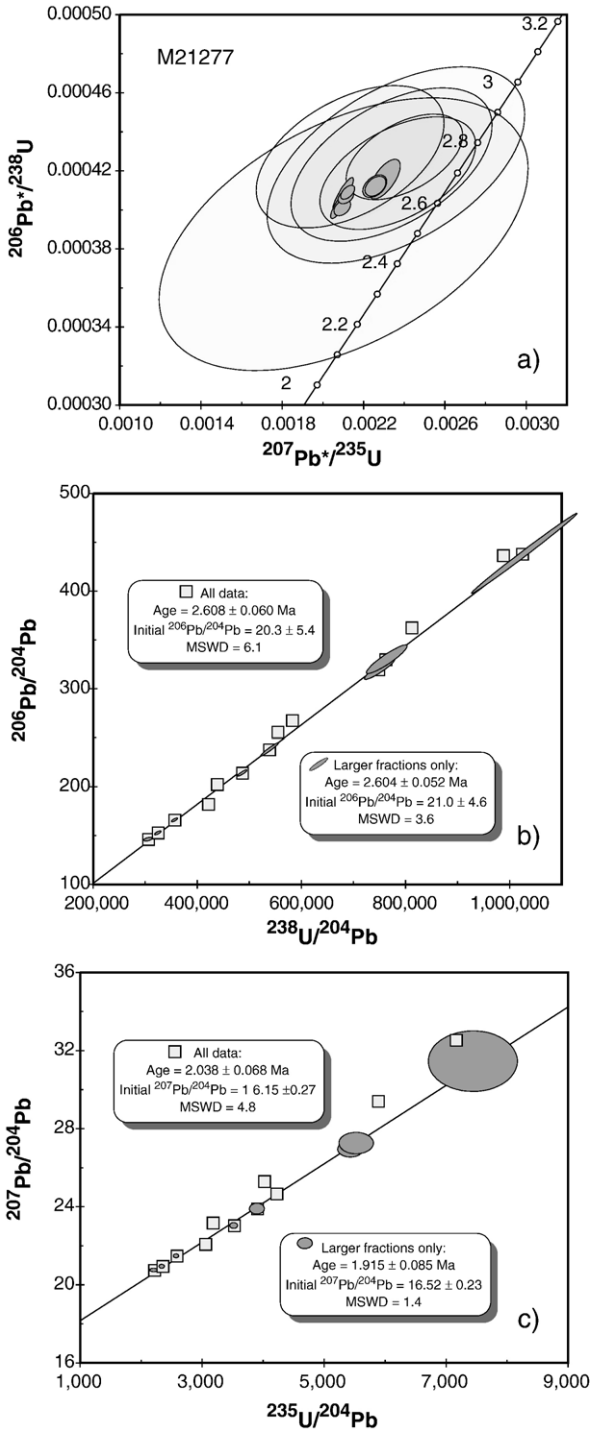

Fig. 7. U–Pb data for the opal M21277. (a) Concordia plot. Error ellipses are 2σ. (b) $^{238}U/^{204}Pb$–$^{206}Pb/^{204}Pb$ and c) $^{235}U/^{204}Pb$–$^{207}Pb/^{204}Pb$ isochron diagrams. In the isochron plots (b, c), error ellipses for relatively imprecise analyses of the smaller fractions (#17–22) are not shown for clarity. All errors and their correlations are reported in Table 3.

sample at the 100–200 μm scale, however these analyses have larger errors due to low intensity of Pb ion beam, and the age resolution is poor. More precise analyses of the larger fractions #23–30 form two groups, which differ by $^{207}Pb*/^{235}U$ and to a lesser degree by $^{206}Pb*/^{238}U$. All three fractions in the group with higher $^{207}Pb*/^{235}U$ have measured $^{206}Pb/^{204}Pb$ between 142 and 162, whereas the fractions in the other group have $^{206}Pb/^{204}Pb$ between 206 and 360. The $^{238}U/^{204}Pb$–$^{206}Pb/^{204}Pb$ and $^{235}U/^{204}Pb$–$^{207}Pb/^{204}Pb$ isochrons (Fig 7b,c) do not show age diversity, such as seen in the concordia diagram. Thus, the grouping of points is probably a result of unusual isotopic composition of initial Pb, rather than of age variations. Indeed, the initial $^{207}Pb/^{204}Pb$ of 16.15–16.52 is higher than in the average continental crust or in any common type of rock (the initial $^{206}Pb/^{204}Pb$ is too imprecise for definitive interpretation). This elevated $^{207}Pb/^{204}Pb$ suggests that the solution from which the opal M21277 precipitated was derived from, or interacted with, an older rock or mineral with high U/Pb ratio that accumulated radiogenic Pb during its lifespan. The $^{238}U/^{204}Pb$–$^{206}Pb/^{204}Pb$ isochron date is older than the $^{235}U/^{204}Pb$–$^{207}Pb/^{204}Pb$ isochron date (Fig. 7 b, c). This relationship holds for regressions of all fractions, and for more precise analyses of larger fractions that yielded less scattered isochrons. This age difference is probably related to the presence of unsupported ^{206}Pb from decay of initial excess ^{234}U and possibly other intermediate decay products of ^{238}U.

U–Pb characteristics of the opal BZ-VV (Fig. 8), uranium content, $^{206}Pb/^{204}Pb$ and $^{207}Pb/^{204}Pb$ ratios, reverse discordance of the U–Pb system, and the age homogeneity, closely resemble the opal M21277. The 2.352±0.085 Ma opal BZ-VV is, however, about 0.44 Ma older than M21277, and the initial $^{207}Pb/^{204}Pb$ derived from the $^{235}U/^{204}Pb$–$^{207}Pb/^{204}Pb$ isochron is consistent within typical crustal values (Kramers and Tolstikhin, 1997).

Four fractions analyzed from the sample HV-1 have moderately low (21–46 ppm) uranium concentrations. This sample contains the least radiogenic Pb among the studied common opals with $^{207}Pb/^{204}Pb$ between 16.9 and 18.4 (Table 3), therefore the $^{207}Pb*/^{235}U$ dates are more sensitive to uncertainty in the initial Pb. Three out of four concordant U–Pb dates are equivalent (Fig. 9a), the fourth fraction appears to be older. However, in the $^{238}U/^{204}Pb$–$^{206}Pb/^{204}Pb$ and $^{235}U/^{204}Pb$–$^{207}Pb/^{204}Pb$ isochron diagrams (Fig. 9b,c), all four analyses plot on the same line. The apparent initial $^{206}Pb/^{204}Pb$=34.5±3.5 and $^{207}Pb/^{204}Pb$=16.33± 0.38 are high and suggest an old, high-U/Pb source for

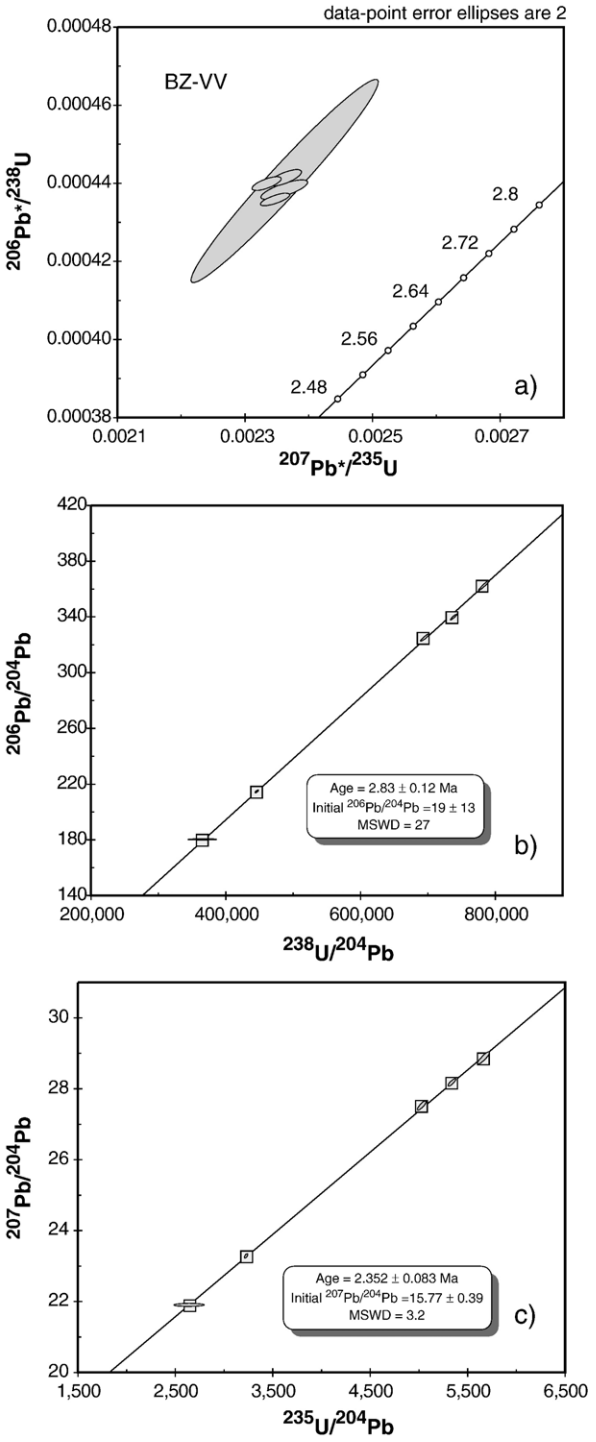

Fig. 8. U–Pb data for the opal BZ-VV. (a) Concordia plot. (b) $^{238}U/^{204}Pb$–$^{206}Pb/^{204}Pb$ isochron diagram. (c) $^{235}U/^{204}Pb$–$^{207}Pb/^{204}Pb$ isochron diagram. Error ellipses are 2σ in all three plots.

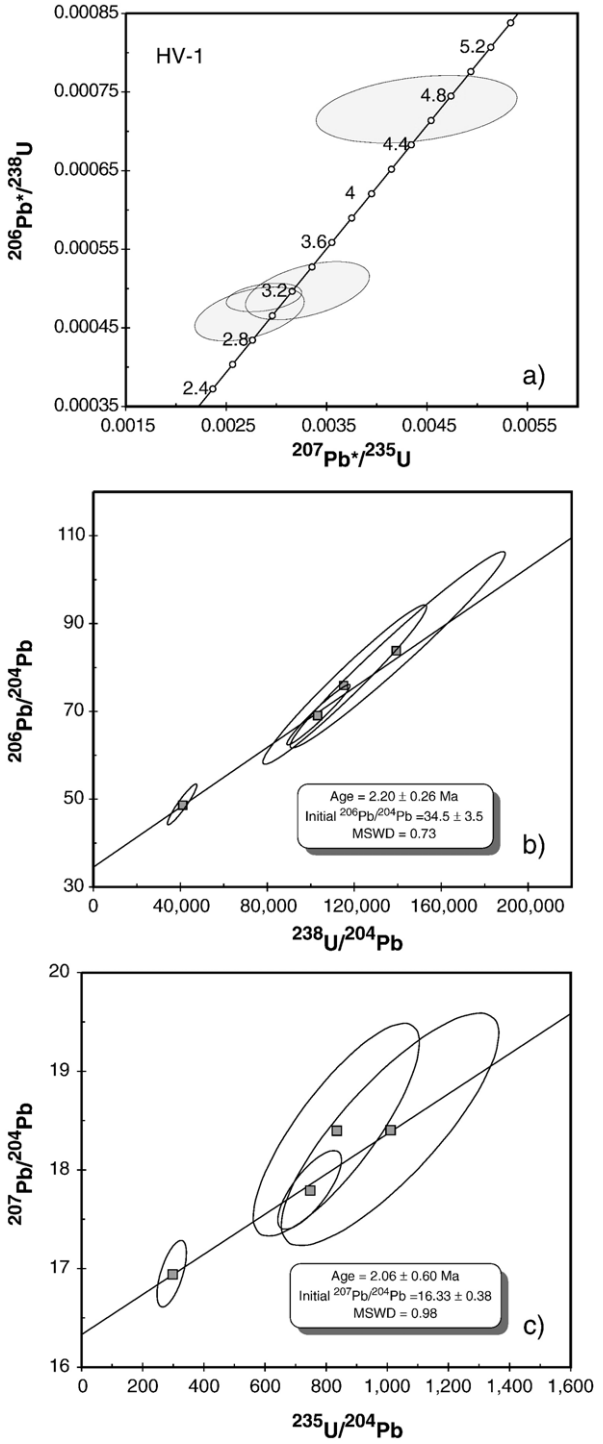

Fig. 9. U–Pb data for the opal HV-1. (a) Concordia plot. (b) $^{238}U/^{204}Pb$–$^{206}Pb/^{204}Pb$ isochron diagram. (c) $^{235}U/^{204}Pb$–$^{207}Pb/^{204}Pb$ isochron diagram. Error ellipses are 2σ in all three plots.

Table 4
U–Th isotopic data

Sample	Fraction # (1)	U ppm	Th ppb	($^{234}U/^{238}U$) (2)	2s %err	($^{230}Th/^{238}U$) (2)	2s %err
E1989	1	7	0.129	1.0033	0.72	0.9985	1.24
	2	2	0.015	0.9910	0.94	0.9903	1.77
	Wtd Aver.			0.9987	0.57	0.9958	0.99
M21006	7	549	36	0.9976	0.47	1.0031	0.53
	12	266	355	0.9978	0.38	1.0005	0.42
	USGS	278	1652	1.0029	0.32	–	–
	USGS	378	1325	1.0041	0.34	0.9995	0.46
	USGS	344	1020	1.0043	0.94	0.9963	0.38
	Wtd Aver.			1.0014	0.39	0.9993	0.44
M21277		859	140	0.9941	0.20	1.0019	0.46
		489	138	1.0001	0.26	1.0096	0.51
	USGS	847	175	1.0050	0.28	–	–
	USGS	928	329	1.0021	0.28	–	–
	USGS	667	204	1.0090	0.27	1.0012	0.62
	Wtd Aver.			1.0008	0.75	1.0040	1.10
BZ-VV	27	841	173	0.9902	0.31	0.9926	0.28
	28	748	228	0.9938	0.68	0.9896	0.20
	30	852	208	0.9915	0.42	0.9905	0.34
	31	888	176	0.9866	0.42	0.9896	0.32
	32	870	68	–	–	0.9969	0.33
	Wtd Aver.			0.9900	0.40	0.9913	0.35

(1) Fraction numbers are keyed to Table 1. Fractions labelled "USGS" were analyzed at USGS for U–Th isotopes only (not analyzed for U–Pb).
(2) Activity ratios, calculated using the decay constants of Jaffery et al. (1971) and Cheng et al. (2000).

the Pb, as discussed above for the opal M21277. The small number of analyses for the opal HV-1 is not sufficient to evaluate whether the apparent age heterogeneity seen in the concordia diagram is real, or if it is caused by the presence of anomalous initial Pb.

All four studied precious opals have much lower U content and $^{238}U/^{204}Pb$ and much higher Pb concentration than any of the common opals (Table 3). Their Pb isotopic compositions are rather uniform and are very close to the model isotopic composition of modern continental crust (Stacey and Kramers, 1975). No U–Pb ages could be calculated from these data.

5.4. ^{230}Th–U data

Multiple ^{230}Th–^{234}U–^{238}U analyses from four common opal samples (Table 4) show that three of them (E1989, M21277, and M21006) have both $^{230}Th/^{238}U$ and $^{234}U/^{238}U$ ratios in secular equilibrium. The activity ratios in BZ-VV are below the equilibrium values by ca. 1%, slightly outside of analytical errors. This may suggest possible recent loss of uranium. However, the effect is small and needs to be confirmed by more precise measurements before inferences about open system behavior can be made.

6. Discussion

6.1. The relationship between structural, geochemical and isotopic characteristics

The studied common opals can be divided into three groups by their degree of crystallinity: the sample E1989 is amorphous (opal-A), the samples M21277 and M21006 show incipient crystallinity (opal-CT); whereas, the sample HV-1 is the most crystalline (it consists of several varieties of micro-crystalline silica). The opal E1989 has the lowest concentration of U, REE and most other trace elements. It is unlikely, however, that this low concentration is related to the low crystallinity, because the opal M21277, the second least crystalline, is the one richest in U and REE. It is more likely that the chemistry of opals with low crystallinity reflects the composition of their parent solutions.

The opals with low crystallinity (E1989, M21277 and M21006) have very high ratio of U to common Pb ($^{238}U/^{204}Pb$). The $^{238}U/^{204}Pb$ ratio in the more crystalline sample HV-1 is much lower, making this sample less suitable for U–Pb dating. This low $^{238}U/^{204}Pb$ ratio may be an initial feature of this opal, for example caused by precipitation from water with low U/Pb ratio, or by higher temperature of the source water, if the solubility

of Pb increases with temperature faster than the solubility of U. Alternatively, it may be a result of aging (Herdianita et al., 2000, Bustillo and Martinez-Frias, 2003, Rodgers et al., 2004), if the increase in crystallinity in the process of aging is accompanied by loss of uranium. If uranium is indeed lost during evolution of opals towards more crystalline structural forms with lower content of water, then radiogenic Pb can also be lost. Since U and Pb loss is not necessarily congruent, the aging can possibly disturb the U–Pb isotopic system. In this case, the degree of crystallinity may suggest preservation or loss of isotopic age information. However, it still remains to be tested, by experimental work or by the study of natural opal occurrences with the gradient of crystallinity and U concentration, whether opals lose U during aging.

6.2. Initial Pb isotopic ratios, and uncertainty of the opal ages and initial $^{234}U/^{238}U$

The uncertainty of initial Pb isotopic composition can cause a serious difficulty in U–Pb dating of opal. This difficulty is illustrated by comparison of $^{206}Pb*/^{238}U$ and $^{207}Pb*/^{235}U$ dates calculated assuming two different initial Pb isotopic compositions: the average modern crustal value of Stacey and Kramers (1975), and the values calculated from internal $^{238}U/^{204}Pb$–$^{206}Pb/^{204}Pb$ and $^{235}U/^{204}Pb$–$^{207}Pb/^{204}Pb$ isochrons (Table 5). For the two samples with relatively radiogenic Pb (E1989 and M21277), the difference can be as large as 20–23% for both $^{206}Pb*/^{238}U$ and $^{207}Pb*/^{235}U$ dates. For the sample with less radiogenic Pb (HV-1), the difference is about 30–50% for the fractions with relatively more radiogenic Pb, and over 100% for the fraction with less radiogenic Pb. In several cases, the difference is well outside of the 2σ error limits. The apparent initial $^{234}U/^{238}U$ ratios, calculated from $^{207}Pb*/^{235}U$ date and measured $^{206}Pb*/^{238}U$ assuming closed system behaviour (Neymark et al., 2000, 2002; Wilson et al., 2003) also vary substantially with the assumed initial Pb isotopic composition (Table 5).

Neither of the two methods for initial Pb correction used here is perfect. The usage of average crustal value for the initial-Pb correction is a rough approximation and can only be acceptable for highly radiogenic Pb, in which the relative amount of initial Pb in total ^{206}Pb and ^{207}Pb is small. Using the initial Pb calculated from isochrons is better justified, but isochrons are open to a different set of problems. First, the isochron model assumes that age and initial Pb isotopic composition are uniform. If either the timing of formation or the initial Pb isotopic composition is variable in a set of samples regressed together, then the isochron can give erroneous readings of the age and initial Pb ratio. The timing of formation can vary if the opal grew slowly, as did opals in Yucca Mountain tuffs (Neymark and Paces, 2000; Neymark et al., 2000; Paces et al., 2004), or if multiple generations of opals coexisting in one sample are not completely separated, as in the sample M21006. The initial Pb isotopic ratios can vary because of mixing of Pb derived from various sources: "normal" crustal Pb leached from silicate rocks, ancient radiogenic Pb leached from old minerals with high $^{238}U/^{204}Pb$ ratio (zircon, titanite, apatite, uranium minerals) or from ancient carbonate rocks, ancient unradiogenic Pb leached from minerals with low $^{238}U/^{204}Pb$ ratio (feldspar, mica, sulphides), and anomalous Pb produced by preferential leaching of intermediate members in uranium decay chains from a high-U material (e.g. uranium minerals or pre-existing opal). Another potential cause of inaccurate initial Pb calculated from a U–Pb isochron is the loss of uranium after formation of the opal. Recent loss of U, proportional to $^{238}U/^{204}Pb$ ratio, increases the slope of the isochron and hence the apparent age, but does not change the initial Pb isotopic ratio. However, if uranium was preferentially lost from the fractions with lower $^{238}U/^{204}Pb$ ratio, the apparent initial Pb isotopic ratio (the *y*-intercept of the isochron) will be too high. The disturbance of the isochrons caused by mixing of multiple components of initial Pb and additionally complicated by loss of U and/or radiogenic Pb can be hard to decipher. Fortunately, these complicating processes produce tight linear correlations only in exceptional cases (e.g. U loss strictly proportional to $^{238}U/^{204}Pb$ ratio), whereas normally they would increase the scatter of data points. The U–Pb isochrons with excess scatter, and the dates and initial Pb values calculated from them, should be interpreted with caution.

6.3. Studied opals as potential standards for geochronometry

This study shows that we need to look for a potential standard among common opals, not among precious opals. Precious opals contain so little U and have so low $U/^{204}Pb$ ratios, that they may preserve Pb isotopic composition of their source materials without measurable addition of radiogenic Pb at least up to a Palaeozoic age. If precious opals are sufficiently stable over time, they may be potentially used for tracing Pb isotopic compositions in ancient aqueous systems, but they are clearly not suitable for U–Pb dating.

All five common opals contain enough U and sufficiently radiogenic Pb to yield precise U–Pb dates. None of the five samples, however, shows the complete

Table 5
U–Pb ages and apparent initial $^{234}U/^{238}U$ activity ratios, calculated using different initial Pb isotopic compositions

Frac. # (1)	Sample	$^{207}Pb/^{235}U$ Age, Ma (2)	$\pm 2\sigma$ Ma (2)	$^{207}Pb/^{235}U$ Age, Ma (3)	$\pm 2\sigma$ Ma (3)	$^{206}Pb/^{238}U$ Age, Ma (2)	$\pm 2\sigma$ Ma (2)	$^{206}Pb/^{238}U$ Age, Ma (3)	$\pm 2\sigma$ Ma (3)	$^{206}Pb/^{238}U$ Age, Ma (2)	$\pm 2\sigma$ Ma (2)	$^{206}Pb/^{238}U$ (3)	$\pm 2\sigma$ % (3)	$234U/^{238}U_{ini}$ Activity (2,4)	$\pm 2\sigma$ (2)	$234U/^{238}U_{ini}$ Activity (3,4)	$\pm 2\sigma$ (3)
1	E1989	15.279	0.089	15.39	0.14	16.165	0.053	15.609	0.080	0.002511	0.33	0.002424	0.51	3.84	0.31	1.94	0.46
2	E1989	15.20	0.33	15.75	0.64	18.36	0.12	15.61	0.30	0.002853	0.64	0.00242	1.9	10.31	0.69	0.9	1.7
3	E1989	15.00	0.75	14.93	0.23	16.67	0.40	16.64	0.23	0.00259	2.4	0.00258	1.4	6.1	2.3	6.2	1.3
4	E1989	15.10	0.88	15.65	0.71	16.59	0.42	13.47	0.37	0.00258	2.5	0.00209	2.7	5.6	2.4	4.9	2.1
5	E1989	15.38	0.61	15.41	0.30	16.12	0.32	15.70	0.21	0.00250	2.0	0.00244	1.3	3.4	1.8	2.1	1.2
6	E1989	15.62	0.61	15.62	0.20	16.39	0.32	16.13	0.18	0.00255	1.9	0.00251	1.1	3.5	1.8	2.8	1.0
17	M21277	2.13	0.74	1.76	0.26	2.50	0.37	2.447	0.116	0.000387	15	0.000380	4.8	2.3	2.0	3.29	0.62
18	M21277	2.43	0.23	2.19	0.10	2.75	0.12	2.721	0.061	0.000427	4.2	0.000422	2.3	2.21	0.65	2.83	0.35
19	M21277	2.37	0.41	2.17	0.14	2.73	0.21	2.701	0.065	0.000423	7.6	0.000419	2.4	2.3	1.2	2.81	0.36
20	M21277	2.17	0.38	1.91	0.15	2.75	0.19	2.719	0.071	0.000427	7.0	0.000422	2.6	3.0	1.1	3.62	0.38
21	M21277	2.40	0.31	2.09	0.13	2.70	0.15	2.659	0.078	0.000419	5.6	0.000413	2.9	2.16	0.85	2.95	0.44
22	M21277	2.39	0.52	2.21	0.19	2.72	0.26	2.700	0.075	0.000423	9.7	0.000419	2.8	2.3	1.5	2.71	0.42
23	M21277	2.291	0.043	1.943	0.094	2.654	0.027	2.615	0.086	0.000412	1.0	0.000406	3.3	2.35	0.15	3.23	0.48
24	M21277	2.155	0.028	2.043	0.053	2.634	0.019	2.622	0.036	0.000409	0.72	0.000407	1.4	2.68	0.11	2.96	0.20
25	M21277	2.337	0.063	1.932	0.114	2.677	0.054	2.632	0.109	0.000415	2.0	0.000408	4.1	2.28	0.30	3.32	0.61
26	M21277	2.110	0.032	1.947	0.053	2.587	0.032	2.569	0.051	0.000401	1.3	0.000399	2.0	2.68	0.18	3.09	0.29
27	M21277	2.145	0.032	1.918	0.066	2.620	0.019	2.595	0.058	0.000407	0.73	0.000403	2.2	2.67	0.11	3.25	0.32
28	M21277	2.131	0.041	1.973	0.059	2.628	0.045	2.610	0.059	0.000408	1.7	0.000405	2.3	2.73	0.25	3.13	0.33
29	M21277	2.288	0.048	1.906	0.103	2.655	0.031	2.612	0.095	0.000412	1.2	0.000405	3.6	2.36	0.17	3.33	0.53
30	M21277	2.128	0.034	1.873	0.070	2.584	0.021	2.555	0.064	0.000401	0.83	0.000396	2.5	2.61	0.12	3.26	0.35
36	HV1	2.93	0.31	1.96	0.53	3.146	0.096	2.16	0.22	0.000488	3.0	0.000335	10	1.93	0.54	1.9	1.2
37	HV1	3.36	0.51	2.46	0.49	3.20	0.19	2.31	0.21	0.000497	6.1	0.000359	8.9	0.9	1.1	0.9	1.2
38	HV1	4.45	0.82	2.01	1.33	4.69	0.23	2.20	0.56	0.000728	4.9	0.000342	25	2.0	1.3	1.9	3.1
39	HV1	2.78	0.45	2.04	0.41	3.01	0.18	2.27	0.17	0.000467	6.0	0.000353	7.6	2.0	1.0	2.0	1.0

(1) Fraction numbers as in the Table 2.
(2) Data reduced using modern crustal initial Pb (Stacey and Kramers, 1975)
(3) Data reduced using initial Pb values calculated from $^{238}U/^{204}Pb$–$^{206}Pb/^{204}Pb$ and $^{235}U/^{204}Pb$–$^{207}Pb/^{204}Pb$ isochrons:
(4) Initial activity ratio calculated from $^{207}Pb*/^{235}U$ age and measured $^{206}Pb*/^{238}U$ assuming closed system behavior.

set of features to qualify for a good standard. The sample BZ-VV comes closest to meeting the requirements. Its isotopic composition is homogeneous, and the uranium content is uniformly high. The main drawback of this sample is the relatively high content of common Pb. A slight deviation from secular equilibrium may be a concern if this material is to be used as a standard in combined U–Pb and U-series studies.

The opal M21277 would also make an acceptable standard, and it is rather abundant. Indeed, it has been already used as a "standard" in U-series and U–Pb ion microprobe studies (Paces et al., 2000; Paces et al., 2004; Nemchin et al., 2006). The high and relatively uniform uranium content is an advantage of this sample. Results for six small fractions also show age homogeneity of this sample at a ~100 μm scale. High content of common Pb is a disadvantage. Anomalous high initial $^{207}Pb/^{204}Pb$ may be a problem, if the initial Pb in this opal is a variable mixture of common Pb and old "radiogenic" Pb.

The sample E1989 has some features that would be desirable in a geochronometric standard: homogeneous $^{207}Pb^*–^{235}U$ dates and very low content of common Pb. The drawback of E1989 is the low and variable content of uranium. This is also a relatively small sample. The usefulness of this opal as a potential standard is additionally compromised by complexity of the $^{238}U–^{206}Pb$ system.

The other two common opal samples, M21006 and HV-1, are not acceptable as U–Pb standards. Indeed, the sample M21006 would make a perfect standard if one could separate its pure "old" and "young" phases. Unfortunately this does not seem to be possible, if one considers close intergrowth of the phases, abundance of microscopic veins of clear opal in translucent matrix, and the large age heterogeneity between seemingly homogeneous fractions of both young and old opal varieties. This sample can make a very good model material for a study of multiple opal growth and substitution, and can be also used as a U-series equilibrium standard. The sample HV-1 is heterogeneous, has rather unradiogenic Pb isotopic composition, and possibly shows age heterogeneity. It is therefore unsuitable as a standard.

7. Search for a better standard

On the basis of results reported here, we can make suggestions for future search for a better opal U–Pb standard. There may be a good chance of finding appropriate standard among large uniform samples of diatomite opal or clear botryoidal opal. It is necessary to watch out for veins and any other visible heterogeneity. Examination of samples in short-wave UV light can provide good indication for the sample homogeneity and approximate content of uranium. Higher brightness and homogeneity of fluorescence are positive signs. Appropriate standards are unlikely to be found among precious opals.

Once the mineralogically suitable opal samples are found, their applicability as U–Pb and U-series standards should be tested by detailed isotopic studies using high-precision isotope dilution methods and high-resolution ion microprobe and partial dissolution techniques.

8. Conclusions

Common opals with low to moderate degree of crystallinity (opal-A to opal-CT) are strongly enriched in uranium relative to other trace elements (e.g. REE) and to common Pb. Precious opals are low in U, contain high concentrations of common Pb, and are not suitable for U–Pb age determinations. Pb isotopic composition in the studied common opals is sufficiently radiogenic to allow dating samples as young as ~2 Ma with both $^{238}U–^{206}Pb$ and $^{235}U–^{207}Pb$ isotopic systems. The U–Pb systems of the opals are not simple, however. Accurate U–Pb dating of the opals is compromised by the presence of unsupported ^{206}Pb, possibly derived from initial excess ^{234}U, by elevated concentrations and possibly anomalous isotopic composition of initial Pb in some samples, and by the coexistence of multiple opal generations of different ages in one sample. The problems related to the initial Pb correction can be solved, in part, by using $^{238}U/^{204}Pb–^{206}Pb/^{204}Pb$ and $^{235}U/^{204}Pb–^{207}Pb/^{204}Pb$ isochrons, which do not require assumption of a certain initial Pb composition, although they still require assumption that the initial Pb isotopic composition is homogeneous. The scattering of data points in the isochron plots suggests that either initial Pb was isotopically heterogeneous, or that the U–Pb isotopic systems were not closed after formation of the opal. The uncertainty of the initial Pb correction can be further reduced by choosing samples with the lowest content of common Pb and higher U, for example by selecting the varieties with brighter UV fluorescence.

None of the five studied common opals appears to be a perfect standard for U–Pb microbeam analysis. However, two out of five opals come sufficiently close to be acceptable as temporary reference materials. Three opals studied for the $^{230}Th–^{234}U–^{238}U$ isotopic systematics are found to be in secular equilibrium and can be used as the standards for microbeam U-series dating. We suggest criteria for further search for a better U–Pb standard.

Acknowledgments

We are most grateful to Leonid Neymark (USGS) for extensive discussions, U-series analyses, for an informal review, and for providing one of the samples. We are grateful to Bob Ramik (ROM) and Bob Zielinski (USGS) for providing us with most samples for this study. Loretta Kwak (USGS) performed ICP-MS analyses in Denver. This paper has been improved by internal review by Otto van Breemen and two anonymous journal reviews. This study has been supported, in part, by NSERC Discovery grant to YA. **[SG]**

References

Amelin, Y., Zaitsev, A., 2002. Precise geochronology of phoscorites and carbonatites: the critical role of U-series disequilibrium in age interpretations. Geochim. Cosmochim. Acta 66, 2399–2419.

Amelin, Y., Ritsk, E.Y., Neymark, L.A., 1997. Geochronological and Nd–Sr–Pb isotopic study of the relationships between mafic magmatites and ultramafic tectonites in the Chaya massif, Baikal-Muya ophiolite belt. Earth Planet. Sci. Lett. 148, 299–316.

Bustillo, M.A., Martinez-Frias, J., 2003. Green opals in hydrothermalized basalts (Tenerife Island, Spain): alteration and aging of silica pseudoglass. J. Non-Cryst. Solids 323, 27–33.

Cheng, H., Edwards, R.L., Hoff, J., Gallup, C.D., Richards, D.A., Asmerom, Y., 2000. The half-lives of uranium-234 and thorium-230. Chem. Geol. 169, 17–33.

Flörke, O.W., Flörke, U., Giese, U., 1984. Moganite: a new microcrystalline silica-mineral. Neues Jahrb. Mineral. Abh. 149, 325–336.

Gaillardet, J., Viers, J., Dupre, B., 2003. Trace elements in river waters. Treatise on Geochemistry. Surface and Ground Water, Weathering, and Soils, vol. 5, pp. 225–272.

Gerstenberger, H., Haase, G., 1997. A highly effective emitter substance for mass spectrometric Pb isotope ratio determinations. Chem. Geol. 136, 309–312.

Graetsch, H., 1994. Structural characteristics of opaline and microcrystalline silica minerals. Silica. Reviews in Mineralogy, vol. 29. Mineralogical Society of America, pp. 209–232.

Herdianita, N., Browne, P.R.L., Rodgers, K.A., Campbell, K.A., 2000. Mineralogical and textural changes accompanying ageing of silica sinter. Miner. Depos. 35, 48–62.

Kramers, J.D., Tolstikhin, I.N., 1997. Two terrestrial lead isotope paradoxes, forward transport modelling, core formation and the history of the continental crust. Chem. Geol. 139, 75–110.

Ludwig, K.R., 2003. Isoplot-Ex version 3.00, a geochronological toolkit for Microsoft Excel. Berkeley Geochronology Center Special Publication, vol. 4. May 30, 2003. 70 pp.

Ludwig, K.R., Lindsey, D.A., Zielinski, R.A., Simmons, K.R., 1980. U–Pb ages of uraniferous opal and implication for the history of beryllium, fluorine, and uranium mineralization at Spor Mountain, Utah. Earth Planet. Sci. Lett. 46, 221–232.

Miehe, G., Graetsch, H., 1992. Crystal structure of moganite: a new structure type of silica. Eur. J. Mineral. 4, 693–706.

Nemchin, A.A., Neymark, L.A., Simons, S.L., 2006. U–Pb SHRIMP dating of uraniferous opals. Chem. Geol. 227, 113–132.

Neymark, L.A., Amelin, Y., 2002. Extreme U–Th–Pb fractionation among hydrogenic fracture-coating minerals in felsic tuffs at Yucca Mountain, Nevada, USA: implications for geochronology. Geochim. Cosmochim. Acta 66 (15A), A552 (abstr.).

Neymark, L.A., Paces, J.B., 2000. Consequences of slow growth for ^{230}Th/U dating of Quaternary opals, Yucca Mountain, NV, USA. Chem. Geol. 164, 143–160.

Neymark, L.A., Amelin, Y., Paces, J.B., 2000. ^{206}Pb–^{230}Th–^{234}U–^{238}U and ^{207}Pb–^{235}U geochronology of Quaternary opal, Yucca Mountain, Nevada. Geochim. Cosmochim. Acta 64, 2913–2928.

Neymark, L.A., Amelin, Y., Paces, J.B., Peterman, Z.E., 2002. U–Pb ages of secondary silica at Yucca Mountain, Nevada: implications for the paleohydrology of the unsaturated zone. Appl. Geochem. 17, 709–734.

Paces, J.B., Neymark, L.A., Persing, H.M., Wooden, J.L., 2000. Demonstrating slow growth rates in opal from Yucca Mountain, Nevada, using microdigestion and ion-probe uranium-series dating, Programs with Abstracts. GSA Annual Meeting, Reno, NV, p. A-259.

Paces, J.B., Neymark, L.A., Wooden, J.L., Persing, H.M., 2004. Improved spatial resolution for U-series dating of opal at Yucca Mountain, Nevada, USA, using ion-microprobe and in-situ microdigestion methods. Geochim. Cosmochim. Acta 68, 1591–1606.

Rodgers, K.A., Browne, P.R.L., Buddle, T.F., Cook, K.L., Greatrex, R. A., Hampton, W.A., Herdianita, N.R., Holland, G.R., Lynne, B.Y., Martin, R., Newton, Z., Pastars, D., Sannazarro, K.L., Teece, C.I. A., 2004. Silica phases in sinters and residues from geothermal fields of New Zealand. Earth-Sci. Rev. 66, 1–61.

Stacey, J.S., Kramers, J.D., 1975. Approximation of terrestrial lead isotope evolution by a two-stage model. Earth Planet. Sci. Lett. 26, 207–221.

Stirling, C.H., Lee, D.-C., Christensen, J.N., Halliday, A.N., 2000. High-precision in situ ^{238}U–^{234}U–^{230}Th isotopic analysis using laser ablation multiple-collector ICPMS. Geochim. Cosmochim. Acta 64, 3737–3750.

Wilson, N.S.F., Cline, J.S., Amelin, Y.V., 2003. Origin, timing, and temperature of secondary calcite-silica mineral formation at Yucca Mountain, Nevada. Geochim. Cosmochim. Acta 67, 1145–1176.

Zielinski, R.A., 1982. Uraniferous opal, Virgin Valley, Nevada: conditions of formation and implications for uranium exploration. J. Geochem. Explor. 16, 197–216.